Self-Assembled Monolayer of L-Cysteine on Au(111): Hydrogen Exchange between Zwitterionic L-Cysteine and Physisorbed Water

Taeho Shin,[†] Keun-Nam Kim,[‡] Chang-Woo Lee,[†] Seung Koo Shin,*[,‡] and Heon Kang*[,†]

School of Chemistry, Seoul National University, Kwanak-ku, Seoul 151-742, South Korea, and Division of Molecular and Life Sciences, Pohang University of Science and Technology, Pohang 790-784, South Korea

Received: March 10, 2003; In Final Form: June 20, 2003

A self-assembled monolayer (SAM) of L-cysteine [$HSCH_2CH(NH_2)COOH$] was prepared on a Au(111) surface by vapor deposition in ultrahigh vacuum and was characterized by techniques of temperature-programmed desorption (TPD), Cs^+ reactive ion scattering (Cs^+ RIS), and low-energy secondary ion mass spectrometry (LESIMS). Analysis of the amino acid functional groups of SAM indicated that L-cysteine molecules exist in the zwitterionic form. Upon physisorption of the D_2O overlayer on the SAM, the $-NH_3^+$ functional group of cysteine readily exchanges their H atoms with D_2O in the temperature range 125−230 K. The H/D exchange of the $-NH_3^+$ group sequentially occurs with D_2O molecules that are directly hydrogen-bonded to the SAM, and the long-range proton transfer to the upper layer water molecules does not occur. Temperature-programmed reaction study and kinetic analysis yielded an activation energy of 13 ± 1 kJ mol^{-1} for the H/D exchange reaction, which suggests proton tunneling as a mechanism.

1. Introduction

Recently, there are increasing research efforts to prepare biological surfaces for the development of biochips and biocompatible materials and for the understanding of biomolecular recognition.[1] One of the useful methods of preparing biological surfaces is to take advantage of self-assembly of an active surfactant that occurs spontaneously on a solid surface to form a self-assembled monolayer (SAM).[2] Among surfactants, organosulfur compounds have been widely used in the formation of SAMs on gold because of high binding affinity of sulfur to gold.[3−7] The most studied, probably best understood system is the SAM of alkanethiols on Au(111) surfaces.[2−7] When preparing biological surfaces, alkanethiols are typically modified in the tail part to contain a bio-linker such as the carboxyl and amino functional groups for the conjugation with biomolecules. Of the 20 naturally occurring amino acids, L-cysteine ($HSCH_2CH(NH_2)COOH$) is such a modified alkanethiol containing not only a thiol group that binds to gold with high affinity but also carboxyl and amino functional groups that can be conjugated with biomolecules. Thus, the SAM of L-cysteine on gold is an attractive system to study.[8−17]

Amino acids commonly exist in nonzwitterionic neutral forms in the gas phase,[18,19] but in zwitterionic forms in the solid phase or aqueous solution.[19,20] For glycine, for instance, the zwitterion formation through intramolecular proton transfer is an endothermic process that requires an activation energy of 61−120 kJ mol^{-1} according to theoretical calculations.[20−23] In the solid phase, the intermolecular proton transfer takes place between the carboxyl and amino groups of neighboring molecules, and the stable zwitterionic form results from electrostatic interactions. In aqueous solution, the zwitterionic form is stabilized by hydrogen bonding with water molecules. When a monolayer film of amino acids is formed on a solid substrate, however, their intermolecular interactions are different from those in the gas phase, solid, or aqueous solution, due to the surface−adsorbate interactions and somewhat restricted intermolecular interactions between adsorbates in two dimensions. In Figure 1, L-cysteine molecules chemisorbed on a gold surface are schematically shown for two chemical states: a zwitterionic dimer formed by intermolecular hydrogen bonding and an unionized neutral form.

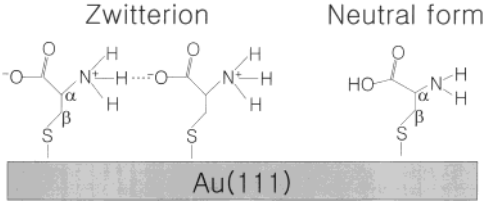

Figure 1. L-Cysteine molecules anchored on a Au(111) surface in a zwitterionic form (left) and a neutral form (right).

The chemical state of L-cysteine on gold has been studied by a number of groups using infrared reflection−absorption spectroscopy (IRAS),[8,9] X-ray photoelectron spectroscopy (XPS),[10−12] secondary ion mass spectrometry (SIMS),[13] and scanning tunneling microscopy (STM).[14−17] Early studies using IRAS by Ihs and Liedberg[8] have suggested two different chemical states for L-cysteine adsorbed from solution. At pH 1.5 and 5.7, L-cysteine binds to gold by the thiol group and exists in a protonated form containing −COOH and $-NH_3^+$ moieties. At pH 11.5, however, it binds to gold by both sulfur and amino nitrogen and exists in a deprotonated form containing $-COO^-$ and $-NH_2$ moieties. Thus, the chemical state of L-cysteine adsorbed on gold from solution is very much correlated to the pH of the solution during adsorption.[9] On the other hand, XPS studies by Uvdal et al.[10] have suggested the zwitterionic state for L-cysteine deposited in a vacuum: L-cysteine forms an organized double layer, with the first layer chemisorbed on gold via the thiol group and the second

* Corresponding authors. (S.K.S.) E-mail: skshin@postech.ac.kr. Fax: +82-54-279-8014. (H.K.) E-mail: surfion@snu.ac.kr. Fax: +82-2-889-1568.
[†] Seoul National University.
[‡] Pohang University of Science and Technology.

10.1021/jp030314j CCC: $25.00
Published on Web 09/27/2003

overlayer physisorbed on the first layer by intermolecular hydrogen bonding between zwitterionic functional groups. Both chemisorbed and physisorbed layers contain the zwitterionic amino acid functional groups, and this zwitterionic state also prevails in the multilayer film. Recently, Cavalleri and co-workers[11,12] have studied L-cysteine adsorbed on a Au(111) surface from solution at pH 5.7 by using XPS and arrived at the same conclusion as Uvdal et al.:[10] L-cysteine is chemisorbed on Au(111) surfaces by a S−Au bond and exists in the zwitterionic state. There are L-cysteine molecules physisorbed on the chemisorbed layer bound by electrostatic interactions. Meanwhile, Legget et al.[13] have analyzed L-cysteine adsorbed on gold from solution at pH 5.7 by SIMS and provided evidence for covalent bond formation between the thiol sulfur atom and gold atoms at the surface. Most recently, Kühnle et al.[17] have observed STM images of D- and L-cysteines adsorbed on Au(110) surfaces by vapor deposition and found that a racemic mixture of D,L-cysteine forms homochiral dimers on Au(110) surfaces. Contrary to popular belief of L-cysteine being in the zwitterionic state, their ab initio density functional theory calculations have indicated that cysteine is in the nonionic state and bound by both sulfur−gold and amino−gold bonds, and the homochiral dimers are held together by intermolecular hydrogen bonding between carboxylic groups.[17] Thus, the chemical state of L-cysteine adsorbed on gold is still elusive and needs to be studied more by using other means.

For a systematic study of L-cysteine chemisorbed on gold, it is desirable to prepare a well-defined and structurally homogeneous monolayer of the molecules. A SAM of L-cysteine formed on a Au(111) surface by vapor deposition in ultrahigh vacuum (UHV) is a good candidate for this purpose. In the present work, we prepared the SAM by this method under careful control of substrate temperature such that the SAM consisted only of the covalently chemisorbed molecules to the surface in the absence of multilayer adsorbates. The chemical state of L-cysteine in the SAM was studied by using Cs^+ reactive ion scattering (RIS)[24] and low-energy secondary ion mass spectrometry (LESIMS).[24−26] In these methods, a sample surface of interest is bombarded with a low-energy (10−100 eV) Cs^+ beam, and the positive ions emitted from the surface are analyzed. The greatest advantages of the techniques are their sensitivity to the first monolayer of the surface and their capability to detect both neutral and ionic adspecies: neutral adspecies are detected in the form of Cs^+−molecule association products (Cs^+ RIS) and the ions by low-energy ion sputtering (LESIMS). The use of low-energy Cs^+ beams suppresses the secondary ionization of neutral molecules and also reduces the damage of surface functional groups.[27,28] These techniques also allow quantitative analysis of isotopically substituted molecules at a surface.[24d,25] Thus, we further analyzed the chemical state of L-cysteine by carrying out H/D exchange reactions of SAMs of L-cysteine with D_2O adsorbed on the SAM in a vacuum. If L-cysteine was in the zwitterionic state, the amine group would exist as the $-NH_3^+$ form, which could exchange hydrogen with deuterium up to three. On the other hand, if it was present in the nonionic state, the neutral $-NH_2$ group would exchange its hydrogen with up to two deuterium and the carboxylic hydrogen would undergo one H/D exchange. The extent of H/D exchange was examined as a function of D_2O exposure, surface temperature, reaction time, and the number of D_2O adsorption−desorption cycles. The activation energy for the H/D exchange process was determined from the temperature dependence of H/D exchange yields, and the H/D exchange mechanism was proposed.

2. Experimental Section

Experiments were carried out in a UHV scattering chamber described previously in detail.[29] In brief, the scattering chamber was equipped with a sample manipulator, a Cs^+ ion gun (Kimball Physics), and a quadrupole mass spectrometer (QMS) (ABB Extrel). Cs^+ ions were produced from surface ionization, and the collision energy was varied in the 10−100 eV range. The Cs^+ current density was 2−3 nA cm^{-2} at the sample. The QMS was used, with its ionizer off, to detect the positive ions scattered from the surface, which include the reflected Cs^+ ions, the Cs^+−neutral molecule association products picked up by Cs^+ at the surface (Cs^+ RIS), and the ions desorbed from the surface by low-energy Cs^+ impact (LESIMS). Since the Cs^+−neutral adducts from Cs^+ RIS appear at masses above Cs^+ at *m*/*z* 133, they are well separated from the LESIMS signals that appear in a mass range lower than the cysteine molecular ion at *m*/*z* 121. The incidence and scattering angles of the beam were varied by rotating a sample and a Cs^+ gun independently around the manipulator axis. A scattering geometry of 60°/60° with respect to the surface normal was typically used for analyzing the sample surface. The QMS was also used for the temperature-programmed desorption (TPD) measurement, but with its ionizer on.

A gold single crystal with an Au(111) face was mounted on a variable-temperature (110−1500 K) stage of a UHV sample manipulator. The gold surface was cleaned by Ar^+ sputtering at 1 keV and annealed at 1000 K. The cleanness of the surface was checked by Cs^+ RIS and LESIMS. L-cysteine (99% purity, Junsei Chemical Co.) was deposited on the Au(111) surface held at 300 K by using a homemade source that was charged with cysteine crystalline powder heated to 400 K. This thermal evaporation temperature is much lower than the decomposing melting point of cysteine at 493 K. The base pressure of the UHV chamber was typically below 1×10^{-10} Torr, and the partial pressure of cysteine was kept within a pressure range $0.5-1.0 \times 10^{-8}$ Torr during deposition. Because the pressure was measured by an ionization gauge located away from the sample, the pressure reading did not accurately represent the vapor pressure near the sample. D_2O (D-enriched to 99.9%, Aldrich) was purified by several freeze−pump−thaw cycles and introduced into the chamber through a metal leak valve. All experiments including SAM preparation, water adsorption, and surface analysis were carried out in situ inside the UHV chamber.

3. Results

3.1. TPD of L-Cysteine and the Preparation of SAM on Au (111). The thermal desorption of L-cysteine deposited on Au(111) at 300 K was examined in a temperature range 300−750 K. The mass spectra were obtained by using a QMS with electron impact ionization at 80 eV. A characteristic mass spectrum of cysteine appears from ∼350 K. As the surface temperature reaches ∼450 K, the intensity of peaks above *m*/*z* 50 decreases sharply, while that of *m*/*z* 34 and 42 peaks increases substantially. Therefore, the TPD of cysteine was monitored at *m*/*z* 121, corresponding to the cysteine molecular ion, and at *m*/*z* 34, corresponding to H_2S^+. Figure 2 shows TPD signals measured at different cysteine exposures. The exposure was deduced from the ionization gauge reading without calibration, and the fresh surface was prepared at each exposure. The cysteine molecular ion appears in a temperature range 353−373 K, and the signal increases as the period of exposure is extended. The appearance of a single desorption peak and its growth with exposure suggest that molecular cysteine desorbs

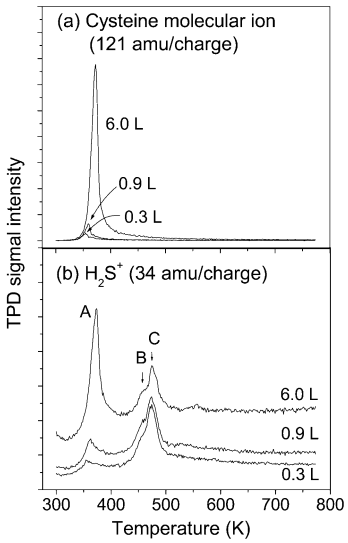

Figure 2. TPD spectra of L-cysteine adsorbed on Au(111) at 300 K. (a) Cysteine molecular ion signal (121 amu/charge). (b) H_2S^+ signal (34 amu/charge). The cysteine exposures are from bottom to top, 0.3, 0.9, and 6.0 L. The exposure was deduced from reading of an ionization gauge distantly located from the sample (see text). The sample heating rate was 3 K/s.

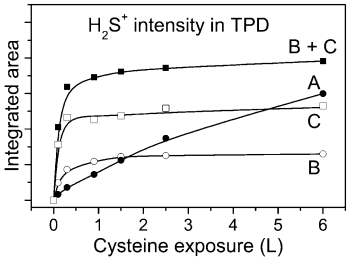

Figure 3. Intensity of H_2S^+ TPD peaks (A, B, and C in Figure 2b) plotted as a function of cysteine exposure in L. The saturation of curve C at 0.3−0.9 L exposure indicates full monolayer coverage of cysteine on Au(111).

from the surface. The peak position shifts slightly to higher temperature with increasing exposure, indicating attractive interactions among cysteine molecules in a multilayer.

Three desorption peaks were observed from the H_2S^+ signal as shown in Figure 2b. The first peak appears at 353−373 K (peak A), and the other two peaks appear at substantially higher temperatures, 458 K (peak B) and 478 K (peak C). Figure 3 shows the intensities of peaks A, B, and C as a function of exposure.

Peak A is very small in the beginning but grows continuously up to 6.0 L, suggesting its multilayer origin. Both the peak position and the growth behavior of A are almost identical to those of the cysteine molecular ion signal shown in Figure 2a. Therefore, peak A is attributed to the desorption of the molecular cysteine which produces the daughter ion at *m*/*z* 34. Note in passing that hydrogen sulfide physisorbed on the Au(111) surface desorbs in a much lower temperature range, 125−165 K.[30] The higher temperature peaks, both B and C, arise sharply in the beginning and then soon become saturated. At these temperatures, no cysteine molecular ion was observed, and the mass spectrum was significantly different from that of the molecular cysteine. In addition, peaks B and C fall into the temperature range where a thermal cleavage of a C−S bond takes place for hexadecanethiol (∼570 K),[3] hexanethiol (∼515 K),[4] and benzenethiol (400−600 K),[5] chemisorbed on Au(111). Therefore, both peaks (B and C) are considered to be derived from thermal decomposition products of cysteine molecules

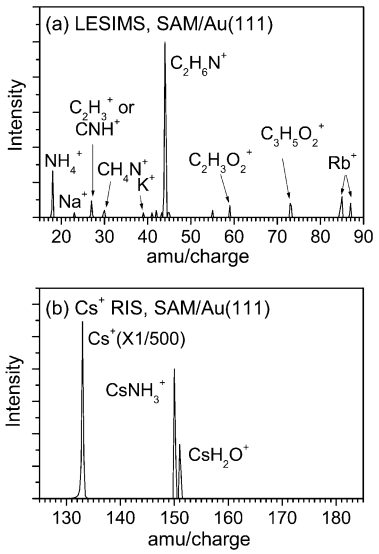

Figure 4. Mass spectrum of LESIMS (a) and that of Cs^+ RIS (b) from the SAM of L-cysteine at 300 K. The Cs^+ impact energy was 50 eV.

TABLE 1: Peak Assignment in the LESIMS and Cs^+ RIS Spectra of L-Cysteine on Au

m/*z*	formula (plausible structure)
18	NH_4^+
27	$C_2H_3^+$ ($CH_2{=}CH^+$)
30	CH_4N^+ ($CH{-}NH_3^+$, $CH_2{=}NH_2^+$)
44	$C_2H_6N^+$ ($CH_2{=}CH{-}NH_3^+$, $CH_3{-}CH{=}NH_2^+$)
55	$C_3H_3O^+$ ($CH_2{=}CH{-}CO^+$, $CH_3{-}C{=}C{=}O^+$)
59	$C_2H_3O_2^+$ ($CH_2{-}COOH^+$, $CH{-}COOH_2^+$)
73	$C_3H_5O_2^+$ ($CH_3{-}CH{-}COOH^+$, $CH_2{=}CH{-}COOH_2^+$)
150	$Cs^+{\cdot}NH_3$
151	$Cs^+{\cdot}H_2O$

chemisorbed on gold through a S−Au linkage. In comparison with B, peak C is more intense, appears at a slightly higher temperature, and becomes saturated at a lower exposure level, which indicates that peak C is related to the more stable adsorption site for cysteine. Since those peaks at 458−478 K are saturated above 0.9 L exposure, this exposure can be used as an upper limit for preparing a monolayer of cysteine on Au(111). In practice, we prepared a cysteine monolayer by dosing a slightly excess amount (≥1 L) of cysteine on Au(111) at 300 K and then desorbing the adsorbates at 373 K for 5 min. This procedure reproduced a cysteine monolayer in a more consistent way, and we called it the "SAM" of cysteine hereafter in order to distinguish it from the cysteine layers produced simply by room-temperature deposition, which may contain some multilayer adsorbates.

3.2. Analysis of SAM by LESIMS and RIS. Surface functional groups of the SAM of L-cysteine were analyzed by LESIMS and Cs^+ RIS techniques. Figure 4a shows an LESIMS spectrum of the ions sputtered from the surface in a lower mass region, whereas Figure 4b depicts a Cs^+ RIS spectrum in a higher mass region. Both spectra were obtained upon 50 eV Cs^+ impact. Table 1 summarizes peaks appearing in Figure 4a,b and their plausible chemical structures.

In the LESIMS spectrum, the two largest signals are $C_2H_6N^+$ (*m*/*z* 44) and NH_4^+ (*m*/*z* 18). The threshold Cs^+ impact energies for these ions are around 20 eV. At such low energies, a majority of the sputtered ions are more likely due to collisional cleavage and ejection of the cationic functional groups preexisting at the surface.[25,26] Secondary ionization of neutral species is less likely to occur under these soft sputtering conditions. $C_2H_6N^+$ may

be ejected by the $C_\beta-S$ and $C_\alpha-C$ bond cleavage, and the plausible structures are $CH_2{=}CH-NH_3^+$ or $CH_3-CH{=}NH_2^+$. NH_4^+ may be produced from the fragmentation of $C_2H_6N^+$ with loss of C_2H_2. Other fragments, such as CH_4N^+ and $C_2H_3^+$, are also considered to be the fragments of $C_2H_6N^+$ with loss of CH_2 and NH_3, respectively. The appearance of $C_2H_6N^+$ and its fragments implies the existence of the protonated amine group ($-NH_3^+$). In addition, the oxygen-containing species, such as $C_3H_5O_2^+$ (*m*/*z* 73), $C_2H_3O_2^+$ (*m*/*z* 59), and $C_3H_3O^+$ (*m*/*z* 55), are observed. However, their intensities are much weaker than $C_2H_6N^+$ or NH_4^+. $C_3H_5O_2^+$ may be derived from the $C_\beta-S$ and $C_\alpha-N$ bond cleavage and subsequent protonation of the fragment, and the plausible structures are $CH_3-CH-COOH^+$ and $CH_2{=}CH-COOH_2^+$. The loss of CH_2 or H_2O from $CH_2{=}CH-COOH_2^+$ results in $C_2H_3O_2^+$ or $C_3H_3O^+$, respectively. The plausible structures for $C_2H_3O_2^+$ are $CH-COOH_2^+$ and CH_2-COOH^+, and those for $C_3H_3O^+$ are $CH_2{=}CH-CO^+$ and $CH_3-C{=}C{=}O^+$. When the LESIMS spectrum is compared with the static SIMS experiments performed using 2 keV Ar^+ beams for L-cysteine chemisorbed on gold,[13] the high-energy SIMS spectrum contains all the peaks in the LESIMS spectrum, along with a variety of peaks that probably arise from the more energetic ion bombardment condition. The alkali-metal ion peaks (Na^+, K^+, Rb^+) in the LESIMS spectrum are attributed to the surface-scattered signals of impurity ions in the Cs^+ beam.

In the Cs^+ RIS spectrum, the scattered Cs^+ primaries appear at *m*/*z* 133 along with the Cs^+-bound RIS products at *m*/*z* 150 and 151. The *m*/*z* 150 and 151 peaks are considered to be $Cs^+{\cdot}NH_3$ and $Cs^+{\cdot}H_2O$, respectively. The $Cs^+{\cdot}NH_3$ signal suggests that neutral NH_3 is expelled from the surface upon ion impact. The expulsion of NH_3 from cysteine has been observed in static SIMS experiments[13] and chemical ionization mass spectrometry.[31] Similarly, $Cs^+{\cdot}H_2O$ indicates liberation of H_2O from the surface, a feature also indicated in the LESIMS spectrum by simultaneous appearance of the $C_3H_5O_2^+$ and $C_3H_3O^+$ peaks.

3.3. H/D Exchange between SAM and Adsorbed D_2O. To further examine the chemical state of the cysteine functional groups on SAM, we investigated the H/D exchange between the SAM and D_2O. If, for instance, the protonated amine groups ($-NH_3^+$) are present on the SAM, the protons will undergo facile H/D exchange with D_2O and the extent of H/D exchange will show up in the isotope patterns of $C_2H_6N^+$ and its fragments. To study the H/D exchange profiles, we covered the SAM surface with D_2O at a submonolayer coverage and then analyzed the surface by LESIMS and Cs^+ RIS techniques. We also carried out the control experiment with a bare Au(111) surface exposed to D_2O vapor at an exposure of 0.3 L at 125 K. The control experiment shows $Cs^+{\cdot}D_2O$ and $Cs^+{\cdot}HDO$ peaks at *m*/*z* 153 and 152, respectively, as given in Figure 5a. The intensity of $Cs^+{\cdot}HDO$ is about 0.15 times the $Cs^+{\cdot}D_2O$ intensity, which indicates the adsorption of HDO impurity, probably generated by H/D scrambling processes inside the stainless steel vacuum chamber. In Figure 5b, D_2O vapor was deposited on the SAM under the same conditions as the control experiment. The relative intensity of $Cs^+{\cdot}HDO$ with respect to $Cs{\cdot}D_2O^+$ becomes twice as big as that of the control experiment, which suggests the occurrence of H/D exchange between SAM and D_2O. When the surface temperature was elevated to 160 K, more pronounced $Cs^+{\cdot}H_2O$ and $Cs^+{\cdot}HDO$ peaks were observed, as shown in Figure 5c, due to the increase in H/D exchange rate with increasing temperature. Note that the $Cs^+{\cdot}$water signal intensity on these water-adsorbed SAM surfaces is stronger than that in Figure 4b by more than 100 times. This is due to an efficient RIS pickup mechanism for physisorbed water molecules,[32] in which the reflecting Cs^+ ions pull the weakly adsorbed molecules via an ion−dipole attraction force even without directly colliding with the adsorbate. Since this is a soft pickup process, the water molecules are lifted up without fragmentation or H/D scrambling.[24d,25] In this respect, the RIS experiment with physisorbed water molecules can probe the SAM surface without destroying the surface functional groups.

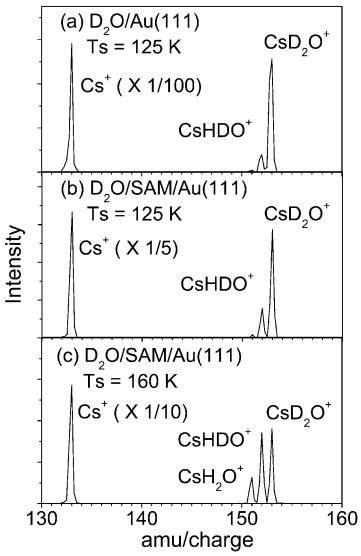

Figure 5. (a) Mass spectrum of Cs^+ RIS from a clean Au adsorbed with D_2O at 125 K for reference. The mass spectra of (b) and (c) were obtained by employing Cs^+ RIS on a D_2O-covered SAM maintained at 125 and 160 K, respectively, after exposure of 0.3 L D_2O onto the SAM at 125 K. The Cs^+ impact energy was 30 eV.

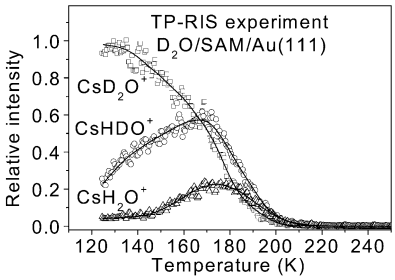

Figure 6. Temperature-programmed Cs^+ RIS (TP-RIS) for a real-time monitoring of CsD_2O^+ (□), $CsHDO^+$ (○), and CsH_2O^+ signals (Δ) on the SAM with increasing temperature (0.5 K/s). The incident Cs^+ beam had an energy of 30 eV with constant intensity during the measurement.

We further investigated the temperature dependence of the H/D exchange profile by using a temperature-programmed RIS (TP-RIS) method. After covering the SAM with D_2O at 125 K, we raised the surface temperature at a speed of 0.5 K/s. $Cs{\cdot}D_2O^+$, $Cs{\cdot}HDO^+$, and $Cs{\cdot}H_2O^+$ peaks were monitored in real time while raising the surface temperature. The intensity of $Cs{\cdot}D_2O^+$ decreases monotonically, while those of $Cs{\cdot}HDO^+$ and $Cs{\cdot}H_2O^+$ peaks increase as shown in Figure 6. The successive appearance of the H/D exchange peaks indicates that the reaction takes place in the following sequence: $D_2O \rightarrow HDO \rightarrow H_2O$. However, these H/D exchange peaks start decreasing above 170 K due to water desorption, and all peaks disappear completely above 230 K.

In the spectra of Figures 5 and 6, the Cs^+ RIS signals of cysteine functional groups were invisible because of the low RIS yield for the SAM buried under the physisorbed water. To analyze the cysteine functional groups, we removed water by heating the surface to 373 K after covering the SAM surface with D_2O at an exposure of 3 L at 140 K. After completely

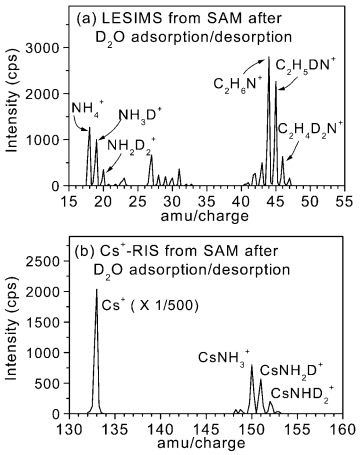

Figure 7. Mass spectrum of LESIMS (a) and that of Cs^+ RIS (b) from the SAM experiencing H/D exchange. D_2O exposure was done at 140 K for 3.0 L. The D_2O-adsorbed SAM was then heated to 373 K to remove the D_2O layer, and the sample temperature was cooled to 300 K for the surface analysis. The Cs^+ impact energy was 50 eV.

desorbing water from the surface, the surface temperature was brought down to 300 K for the analysis. The recovered SAM surface thus has experienced intermolecular interactions with D_2O and undergone H/D exchange reactions over a wide temperature range up to the point of water desorption (<230 K). Figures 7a and b show the LESIMS and RIS spectra, respectively, obtained after such D_2O adsorption−desorption treatments. The LESIMS spectrum revealed sizable peaks at *m*/*z* 18−20, 27−30, and 44−47. Those peaks at *m*/*z* 18−20 must be related to the NH_4^+ peak assigned in Figure 4 in the absence of H/D exchange reactions. They are attributed to NH_4^+, NH_3D^+, and $NH_2D_2^+$, respectively. In the *m*/*z* 27−31 mass range, two peaks at *m*/*z* 27 and 30 were observed in the absence of H/D exchange reactions; however, five sizable peaks were detected as a result of the H/D exchange processes. The isotope patterns in the *m*/*z* 44−47 mass range suggest that $C_2H_6N^+$ exchanges H/D at least three times. The isotope distribution of $NH_{4-x}D_x^+$ ($x = 0-2$) is similar to that of $C_2H_{6-x}D_xN^+$ ($x = 0-2$).

The H/D exchange patterns also appeared in the RIS spectrum: three sizable peaks were observed at *m*/*z* 150, 151, and 152, which can be assigned as $Cs^+ \cdot NH_3$, $Cs^+ \cdot NH_2D$, and $Cs^+ \cdot NHD_2$, respectively. The isotope distribution of $Cs^+ \cdot NH_{3-x}D_x$ ($x = 0-2$) peaks resembles that of $NH_{4-x}D_x^+$ ($x = 0-2$) or $C_2H_{6-x}D_xN^+$ ($x = 0-2$) observed in the LESIMS spectra, suggesting that they are derived from the same origin. $Cs \cdot H_2O^+$ and $Cs \cdot HDO^+$ could decorate those peaks at *m*/*z* 151 and 152 in the RIS spectrum if the $Cs \cdot H_2O^+$ peak in Figure 4 has undergone a H/D exchange reaction.

To summarize, both LESIMS and RIS spectra show that the H/D exchange takes place in the nitrogen-containing signals related to the protonated amine group. The H/D exchange occurs sequentially, replacing up to two hydrogen atoms in these signals and in some cases up to three in a small yield, when a submonolayer coverage of D_2O is supplied to the SAM.

3.4. Effect of D_2O Exposure on the H/D Exchange of SAM. To examine the effect of water thickness on the H/D exchange, we repeated the H/D exchange experiment by varying the exposure of D_2O from 0 to 12 L. The variation of $NH_{4-x}D_x^+$ ($x = 0-3$) intensities is plotted in Figure 8 as a function of D_2O exposure.

At each exposure, D_2O was deposited on a separate, freshly prepared SAM surface at 140 K, and then the D_2O layer was

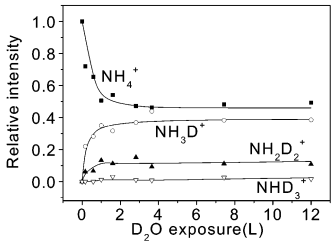

Figure 8. Relative isotopic distribution of the $NH_{4-x}D_x^+$ ($x = 0-3$) signals as a function of D_2O exposure. Each exposure was done on a freshly prepared SAM surface at 140 K. The D_2O-adsorbed SAM surface was heated to 373 K to remove the D_2O layer and then kept at 300 K during the surface analysis. The Cs^+ impact energy was 50 eV.

removed by elevating the surface temperature to 373 K. The SAM surface was analyzed by LESIMS and RIS after the sample temperature was brought down to 300 K. The relative intensities of NH_4^+, NH_3D^+, and $NH_2D_2^+$ reach the steady state at 1 L and remain almost constant up to 12 L. NHD_3^+ is barely detectable in the entire range. Likewise, the relative intensities of $C_2H_{6-x}D_xN^+$ and $Cs \cdot NH_{3-x}D_x^+$ (not shown) also exhibit steady-state isotope patterns. This result suggests that the H/D exchange takes place between the SAM and the D_2O molecules in the first monolayer that are in physical contact with the SAM. Evidently, the D_2O molecules in the upper layer do not participate in H/D exchange reactions. Since the reaction time allowed in these experiments might have been a limiting factor in H/D exchange processes, we prolonged the reaction time up to 1 h and analyzed the surface. We prepared a fresh SAM, deposited a thick D_2O overlayer (7 L) at 140 K, waited for a certain reaction time at 140 K, desorbed water by heating the surface up to 373 K, and then monitored the LESIMS signals for $NH_{4-x}D_x^+$ at 300 K. The isotopic patterns of $NH_{4-x}D_x^+$ were identical to those in Figure 8. They just did not change with reaction time up to 1 h. This result substantiates that the H/D exchange reaction is a localized event taking place at the interface between the SAM and the physisorbed D_2O overlayer. It also indicates that the spontaneous mixing of water does not occur at 140 K or during the desorption period.

To further investigate the localized nature of the H/D exchange reaction, we treated the SAM with multiple D_2O adsorption−desorption cycles, so as to rehydrate the SAM with fresh D_2O molecules at each adsorption−desorption cycle with an exposure of about 3 L. Figure 9 shows the variation of $NH_{4-x}D_x^+$ ($x = 0-3$) and $C_2H_{6-x}D_xN^+$ ($x = 0-3$) obtained from the LESIMS spectra as a function of D_2O adsorption−desorption cycle.

The relative population of NH_4^+ continually decreases and eventually drops to almost zero after 7 cycles, whereas that of singly substituted NH_3D^+ reaches a maximum after 1 or 2 cycles and starts decreasing after 3 cycles. The relative population of doubly substituted $NH_2D_2^+$ keeps growing with increasing adsorption−desorption cycles. Meanwhile, the triply substituted NHD_3^+ signal, which was barely detectable after 1 cycle, gradually increases. The variation of $NH_{4-x}D_x^+$ ($x = 0-3$) signals follows the kinetics of sequential H/D exchange reactions on going from NH_4^+ to NHD_3^+. The variation of $C_2H_{6-x}D_xN^+$ ($x = 0-3$) signals also reveals the sequential reaction kinetics on going from $C_2H_6N^+$ to $C_2H_3D_3N^+$.

The LESIMS and RIS spectra obtained after 7 D_2O adsorption−desorption cycles are shown in Figure 10a and b, respectively. Here again, the isotope patterns show extensive deuterium enrichment in $NH_{4-x}D_x^+$, $C_2H_{6-x}D_xN^+$, and $Cs^+ \cdot NH_{3-x}D_x$ ($x = 0-3$). Importantly, however, these signals indicate that quadruple substitution of deuterium is negligible.

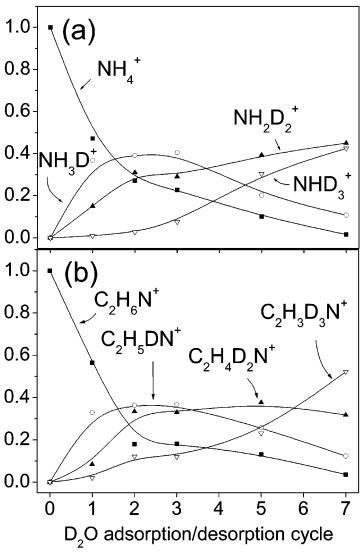

Figure 9. Relative isotopic distribution of the $NH_{4-x}D_x^+$ ($x = 0-3$) signals as a function of the repeated cycles of D_2O exposure (at 140 K)/desorption (at 373 K). The D_2O exposure in each cycle was 2.8 L. The Cs^+ impact energy was 50 eV.

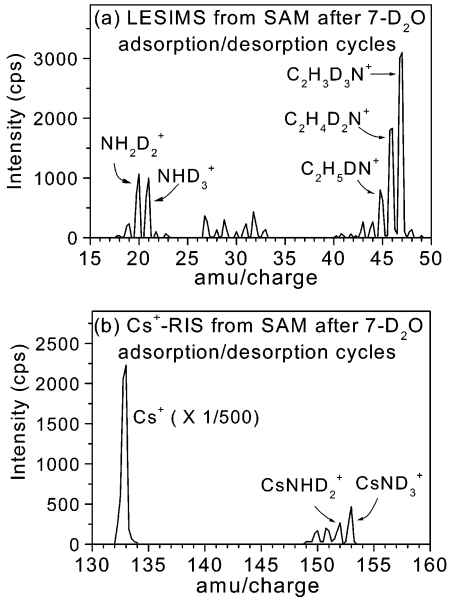

Figure 10. Mass spectrum of LESIMS (a) and that of Cs^+ RIS (b) from the SAM after 7 D_2O adsorption−desorption cycles. D_2O exposure was done for 3.0 L at 140 K, desorption at 373 K, and surface analysis at 300 K. The Cs^+ impact energy was 50 eV.

The small peak at *m*/*z* 48 can be the carbon-13 isotope of *m*/*z* 47 rather than $C_2H_2D_4N^+$. ND_4^+ was observed in small intensity, but this amount of species could easily be formed if the $-ND_3^+$ moiety underwent some recombinative reactions during the sputtering event. The spectral features confirm that the protonated amine group is present on the SAM as an H/D exchange site, and the repeated supply of fresh D_2O molecules can substitute eventually all three hydrogen atoms with deuterium in the protonated amine group.

4. Discussion

4.1. Chemical State of L-Cysteine in SAM. The TPD result presented in section 3.1 reveals that the SAM prepared by vacuum deposition at 373 K consists of a monolayer of L-cysteine molecules chemisorbed on the Au(111) surface through a S−Au bond, which is free of the multiplayer adsorbates physisorbed on top of the monolayer by intermolecular hydrogen bonding. In the SAM, L-cysteine molecules could exist in either the zwitterionic form or the neutral form, or both. We will discuss each of these possibilities in light of the LESIMS and RIS results.

If the zwitterionic form was present at the surface, the low-energy Cs^+ impact would produce fragment ions that contain the $-NH_3^+$ moiety, such as $C_2H_6N^+$ (*m*/*z* 44) and NH_4^+ (*m*/*z* 18), which were observed in the present study. These NH_3^+-containing peaks were deuterated up to three upon H/D exchange reactions with D_2O, supporting the existence of the $-NH_3^+$ group. Collisional cleavage of the $C_\alpha-COO^-$ bond in the zwitterionic molecules would produce anionic COO^- or neutral $CsCO_2$. These species, however, would not be detected in the present experiment monitoring only positive ions. The other peaks seen in the LESIMS spectra are $C_3H_3O^+$ (*m*/*z* 55), $C_2H_3O_2^+$ (*m*/*z* 59), and $C_3H_5O_2^+$ (*m*/*z* 73). The sputtering mechanisms leading to these species are not obvious, but they have also been observed[13] in the static SIMS spectra of L-cysteine chemisorbed on gold or in a crystalline form, in the latter the molecules certainly being in the zwitterionic state. In the RIS spectra, $Cs^+ \cdot NH_3$ (*m*/*z* 150) could be formed if NH_3 was expelled from the zwitterionic molecules, and this phenomenon has been known in static SIMS[13] and chemical ionization mass spectrometry studies.[31] These considerations conclude that the LESIMS and RIS features are consistent with the presence of zwitterionic cysteine in the SAM.

If L-cysteine existed in the neutral form, the Cs^+ impact at the surface would have cleaved the $C_\alpha-NH_2$, $C_\alpha-COOH$, or $OC-OH$ bond, and this cleavage would have produced RIS products of $Cs^+ \cdot NH_2$, $Cs^+ \cdot COOH$, or $Cs^+ \cdot OH$, respectively. These signals, however, were not observed in the RIS measurement. This is negative evidence against the neutral form, and since there is no positive evidence that exclusively supports the neutral form, we are forced to consider that the SAM did not contain neutral cysteine molecules. Nevertheless, one could still imagine that the Cs^+ impact transiently transformed the cysteine molecules from a neutral to a zwitterionic form via intramolecular proton transfer. If this happened, the neutral molecules would yield the same results in the spectra as for the zwitterionic form.

The water adsorption experiments give an additional hint for the chemical state issue. If the neutral functional groups existed at the surface, they would be subjected to change upon water adsorption. The intermolecular interactions between the adsorbed water molecules and the neutral functional groups would change the chemical state to a monomeric, intramolecular zwitterionic form, somewhat like the situation occurring in aqueous solution. The subsequent desorption of water from the SAM would then evaporate the hydrogen-bond interactions between water and amino acid functional groups and cause the zwitterionic monomers to change to zwitterionic dimers (or multimers), the latter being stabilized by lateral intermolecular hydrogen bonding as depicted in Figure 1. This scenario assumes irreversible conversion of the neutral form in the absence of water to the more stable, zwitterionic dimer (or multimer) by a water adsorption−desorption process. In the LESIMS experiment, we observed that the $C_2H_6N^+$ (*m*/*z* 44) and NH_4^+ (*m*/*z* 18) signals, which originated from zwitterionic cysteine, did not noticeably increase in intensity by the water adsorption−desorption process. The threshold energies for producing these signals did not change either. This shows that the amount of the $-NH_3^+$ functional group at the surface did not increase by the water

treatment procedure, which implies that the neutral form of cysteine was very scarce or absent in the originally prepared SAM.

4.2. Mechanism of the H/D Exchange: Proton Tunneling. We have shown in Figures 9 and 10 that the $-NH_3^+$ group in the zwitterionic form sequentially exchanges up to three H atoms with adsorbed D_2O molecules. Moreover, Figure 8 reveals that the H/D exchange occurs at the interface of the SAM and the water overlayer, presumably via a reversible proton transfer between the $-NH_3^+$ group and hydrogen-bonded D_2O molecules. Thermal diffusion and/or spontaneous mixing of the adsorbed water molecules occur insignificantly. The nonoccurrence of the mixing of water molecules within the overlayer is consistent with the results of isotope exchange experiments done with nanocrystals[33] or thin films of pure water−ice.[34] On the other hand, when the ice sample is enriched with protons by doping with HCl, the H/D exchange activity is greatly enhanced to be observable even at 110 K.[33] The implication of this excess proton effect for the present finding is that when the $-NH_3^+$ and the $-COO^-$ functional groups exist together, they as a whole may not be an effective proton donor, since they scarcely enhance the H/D exchange activity of the water molecules in the upper layers.

In the following, we analyzed the kinetics of the H/D exchange process observed from the TP-RIS experiment (Figure 6) using a kinetic model. The model consists of two H/D exchange processes occurring in sequence between the protonated amine group and the hydrogen-bonded water molecule (eqs 1 and 2).

$$-NH_3^+\cdots D_2O \underset{k_{-1}}{\overset{k_1}{\rightleftharpoons}} -NH_2D^+\cdots HDO \qquad (1)$$

$$-NH_2D^+\cdots HDO \underset{k_{-2}}{\overset{k_2}{\rightleftharpoons}} -NHD_2^+\cdots H_2O \qquad (2)$$

Here, $-NH_3^+\cdots D_2O$ denotes a hydrogen-bonded pair of the $-NH_3^+$ group and D_2O. We assume that the water molecule does not diffuse out during H/D exchange and remains in contact with the hydrogen-bonded $-NH_3^+$ group. We chose reaction 2 to fit the experimental data rather than reaction 1, because the experimental D_2O signal contains some amounts of D_2O adsorbed on bare Au sites at low temperature. The rate expression for reaction 2 can be written as eq 3.

$$\frac{d[-NHD_2^+\cdots H_2O]}{dt} = k_2[-NH_2D^+\cdots HDO] - k_{-2}[-NHD_2^+\cdots H_2O] \qquad (3)$$

where k_2 and k_{-2} are the forward and reverse rate constants, respectively. The details of the derivation of necessary kinetic equations and analysis procedures are given in the Appendix. Equation A4 in the Appendix allows us to make an Arrhenius plot from the data of Figure 6. Figure 11 shows the plot in the temperature range 140−160 K. From the slope of a linear fit, we obtained an activation energy of 13 ± 1 kJ mol^{-1} for the H−D exchange process.

For a proton-transfer reaction between NH_4^+ and H_2O in aqueous solution to form hydronium ion and ammonia, the products lie 50 kJ mol^{-1} above the reactants.[35] In the gas phase, the energy difference increases to 171 kJ mol^{-1}.[36] When compared with these values, the measured activation energy of 13 kJ mol^{-1} is very small, indicating that the H/D exchange in the present case does not involve a hydronium ion intermediate. The hydronium ion state would be able to be stabilized at the surface by the neighboring $-COO^-$ group, but this effect would probably not reduce the classical barrier height (the saddle-point energy on the potential energy surface) to a value as low as 13 kJ mol^{-1}. Thus, the very small activation energy measured in this work denies the possibility of hydronium ion formation via a proton transfer, but suggests the direct proton exchange via proton tunneling between the $-NH_3^+$ group and the water molecule.

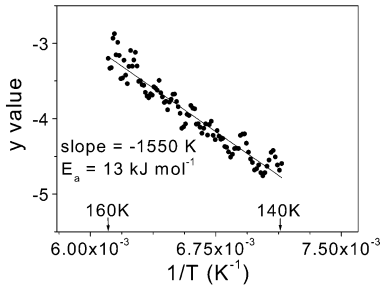

Figure 11. Arrhenius plot for the activation energy of H/D exchange reaction. The *y*-value corresponds to $\ln[dI(CsH_2O^+)/dT] - \ln[I(CsHDO^+) - 2I(CsH_2O^+)]$ (see Appendix for the related equations).

5. Conclusion

In this work, a SAM of L-cysteine was prepared on Au(111) by temperature-controlled vacuum deposition, and the hydrogen exchange between the SAM and the adsorbed water was examined by techniques of TPD, LESIMS, Cs^+ RIS, and TP-RIS. The conclusions drawn from this investigation can be summarized as follows.

(i) L-Cysteine molecules in the SAM exist in the zwitterionic form, which is stabilized by intermolecular hydrogen bonding, according to the results of the LESIMS and RIS analyses of the end functional groups. The RIS and water adsorption−desorption experiments provided negative evidence against the existence of the neutral form in any appreciable amount. The SAM may contain zwitterionic molecules exclusively. Thus, zwitterionic functional groups are the chemically active sites for the conjugation with biomolecules on the SAM.

(ii) The $-NH_3^+$ group of L-cysteine readily exchanges hydrogen with physisorbed D_2O molecules even at low temperatures (125−230 K). The H/D exchange sequentially occurs with D_2O molecules that are directly hydrogen-bonded to the SAM. The H/D exchange does not propagate to water molecules in the upper physisorbed layers.

(iii) Kinetic analysis of the temperature-dependent H/D exchange reaction provided an activation energy of 13 ± 1 kJ mol^{-1} for the reaction, which suggests proton tunneling between the $-NH_3^+$ group and the D_2O molecule.

A unique feature of the present work is that the H/D exchange between an amino acid and water was examined at a simple and well-defined interface composed of a SAM and a physisorbed water layer. This allowed the H/D exchange to be probed by the surface analysis tools with a monolayer depth resolution of the water layer under the control of water coverage and reaction temperature. The interfacial conditions prepared in this work must be quite different from those in aqueous solution, for which many aspects are still uncertain to the molecular detail. Nevertheless, the present findings might be used as an interesting reference for a more systematic solution study of the H/D exchange process.

Acknowledgment. We thank Dr. Yong-Wook Kim for his guidance in RIS instrumentation. The project was supported by the Basic Research Program of the Korea Science & Engineering

Foundation (R02-2002-000-00005-0). S.K.S. acknowledges support from the Basic Science Research Institute at POSTECH and the Brain Korea 21 Program.

Appendix

The rate expression for the H/D exchange between $-NH_2D^+$ and HDO (eq 2) has been given by eq 3 in section 4.2. In reaction 2, both reactants and products have identical H or D atoms. Due to the presence of identical atoms, the forward reaction path is doubly degenerate and the backward reaction quadruply degenerate. In the following we considered a single H−D exchange step for which the reaction multiplicity was removed, and we assigned its rate constant as k. From considerations of the reaction degeneracy and symmetry in the forward and backward reactions, $k_2 = 2k$ and $k_{-2} = 4k$. As long as the ammonium group and the water molecule remain in contact as a pair, the concentrations $[-NH_2D^+\cdots HDO]$ and $[-NHD_2{}^+\cdots H_2O]$ in eq 3 can be replaced with [HDO] and $[H_2O]$, respectively, leading to eq A1.

$$d[H_2O]/dt = 2k[HDO] - 4k[H_2O] \quad \text{(A1)}$$

[HDO] and $[H_2O]$ are again directly proportional to the corresponding RIS signal intensities, $I(CsHDO^+)$ and $I(CsH_2O^+)$.

$$dI(CsH_2O^+)/dt = 2k[I(CsHDO^+) - 2I(CsH_2O^+)] \quad \text{(A2)}$$

The heating rate in the TP-RIS experiment is $\beta = dT/dt$, and $k = A\exp(-E_a/RT)$, where E_a is the activation energy. Inserting these relationships into eq A2 leads to eq A3.

$$\beta\, dI(CsH_2O^+)/dT = 2A\exp(-E_a/RT)[I(CsHDO^+) - 2I(CsH_2O^+)] \quad \text{(A3)}$$

Taking a natural logarithm and rearranging eq A3 results in eq A4.

$$\ln[dI(CsH_2O^+)/dT] - \ln[I(CsHDO^+) - 2I(CsH_2O^+)] = -(E_a/R)(1/T) + \text{const.} \quad \text{(A4)}$$

Equation A4 can be used to make an Arrhenius-type plot from the data in Figure 6. The RIS intensities are taken from raw kinetic data, and the derivative, $dI(CsH_2O^+)/dT$, is obtained from the curve fitting in Figure 6.

References and Notes

(1) Kasemo, B. *Surf. Sci.* **2002**, *500*, 656.
(2) Ulman, A. *Chem. Rev.* **1996**, *96*, 1533.
(3) Nuzzo, R. G.; Dubois, L. H.; Allara, D. L. *J. Am. Chem. Soc.* **1990**, *112*, 558.
(4) Kondoh, H.; Kodama, C.; Nozoye, H. *J. Phys. Chem. B* **1998**, *102*, 2310.
(5) Whelan, C. M.; Barnes, C. J.; Gregoire, C.; Pireaux, J.-J. *Surf. Sci.* **2000**, *454*, 67.
(6) Poirier, G. E.; Pylant, E. D. *Science* **1996**, *272*, 1145.
(7) Grönbeck, H.; Curioni, A.; Andreoni, W. *J. Am. Chem. Soc.* **2000**, *122*, 3839.
(8) Ihs, A.; Liedberg, B. *J. Colloid Interface Sci.* **1991**, *144*, 282.
(9) Uvdal, K.; Vikinge, T. P. *Langmuir* **2001**, *17*, 2008.
(10) Uvdal, K.; Bodö, P.; Liedberg, B. *J. Colloid Interface Sci.* **1992**, *149*, 162.
(11) Dodero, G.; De Michieli, L.; Cavalleri, O.; Rolandi, R.; Oliveri, L.; Daccà, A.; Parodi, R. *Colloids Surf.* **2000**, *175*, 121.
(12) Cavalleri, O.; Oliveri, L.; Daccà, A.; Parodi, R.; Rolandi, R. *Appl. Surf. Sci.* **2001**, *175*−*176*, 357.
(13) Leggett, G. J.; Davies, M. C.; Jackson, D. E.; Tendler, J. B. *J. Phys. Chem.* **1993**, *97*, 5348.
(14) Dakkouri, A. S.; Kolb, D. M.; Edelstein-Shima, R.; Mandler, D. *Langmuir* **1996**, *12*, 2849.
(15) Zhang, J.; Chi, Q.; Nielsen, J. U.; Friis, E. P.; Andersen, J. E. T.; Ulstrup, J. *Langmuir* **2000**, *16*, 7229.
(16) Xu, Q.-M.; Wan, L.-J.; Wang, C.; Bai, C.-L.; Wang, Z.-Y.; Nozawa, T. *Langmuir* **2001**, *17*, 6203.
(17) Kühnle, A.; Linderoth, T. R.; Hammer, B.; Besenbacher, F. *Nature* **2002**, *415*, 891.
(18) Albrecht, G.; Corey, R. B. *J. Am. Chem. Soc.* **1939**, *61*, 1087.
(19) Jensen, J. H.; Gordon, M. S. *J. Am. Chem. Soc.* **1995**, *117*, 8159.
(20) Jonsson, P. G.; Kvick, A. *Acta Crystallogr. B* **1972**, *28*, 1827.
(21) Tse, Y.-C.; Newton, M. D.; Vishveshwara, S.; Pople, J. A. *J. Am. Chem. Soc.* **1978**, *100*, 4329.
(22) Tuñón, I.; Silla, E.; Ruiz-López, M. F. *Chem. Phys. Lett.* **2000**, *321*, 433.
(23) Grabowski, S.; Krygowski, T. M.; Stepien, B. *J. Phys. Org. Chem.* **2000**, *13*, 740.
(24) Yang, M. C.; Hwang, C.-H.; Kang, H. *J. Chem. Phys.* **1997**, *107*, 2611. (b) Kang, H.; Yang, M. C.; Kim, K.-D.; Kim, K.-Y. *Int. J. Mass Spectrom. Ion Processes* **1998**, *174*, 143. (c) Kim, K.-Y.; Shin, T.-H.; Han, S.-J.; Kang, H. *Phys. Rev. Lett.* **1999**, *82*, 1329. (d) Kim, C. M.; Hwang, C.-H.; Lee, C.-W.; Kang, H. *Angew. Chem., Int. Ed.* **2002**, *41*, 146.
(25) Park, S.-C.; Maeng, K.-W.; Pradeep, T.; Kang, H. *Angew. Chem., Int. Ed.* **2001**, *40*, 1497.
(26) Kang, H.; Shin, T.-H.; Park, S.-C.; Kim, I. K.; Han, S.-J. *J. Am. Chem. Soc.* **2000**, *104*, 552.
(27) Kasi, S. R.; Kang, H.; Sass, C. S.; Rabalais, J. W. *Surf. Sci. Rep.* **1989**, *10*, 1.
(28) Cooks, R. G.; Ast, T.; Pradeep, T.; Wysocki, V. *Acc. Chem. Res.* **1994**, *27*, 316.
(29) Han, S.-J.; Lee, C.-W.; Hwang, C.-H.; Lee, K.-H..; Yang, M. C.; Kang, H. *Bull. Korean Chem. Soc.* **2001**, *22*, 883.
(30) Leavitt, A. J.; Beebe, T. P., Jr. *Surf. Sci.* **1994**, *314*, 23.
(31) Milne, G. W. A.; Axenrod, T.; Fales, H. M. *J. Am. Chem. Soc.* **1970**, *92*, 5170.
(32) Hahn, J. R.; Lee, C. W.; Han, S.-J.; Lahaye, R. J. W. E.; Kang, H. *J. Phys. Chem. A* **2002**, *106*, 9827.
(33) Uras-Atemiz, N.; Joyce, C.; Devlin, J. P. *J. Chem. Phys.* **2001**, *115*, 9835.
(34) Everest, M. A.; Pursell, C. J. *J. Chem. Phys.* **2001**, *115*, 9843.
(35) Gibbs free energy calculated from $K_{eq} = 6 \times 10^{-10}$ for the reaction $H_3O^+ + NH_3 \leftrightarrow H_2O + NH_4^+$.
(36) Calculated from the gas-phase proton affinity: $PA(H_2O) = 695$ kJ mol^{-1}, $PA(NH_3) = 866$ kJ mol^{-1}.